RESEARCH ARTICLE

Influence of pulse sequence parameters at 1.5 T and 3.0 T on MRI artefacts produced by metal–ceramic restorations

[1,2]A R G Cortes, [3]R Abdala-Junior, [3]M Weber, [3]E S Arita and [1,2]J L Ackerman

[1]Martinos Center for Biomedical Imaging, Department of Radiology, Massachusetts General Hospital, Charlestown, MA, USA; [2]Department of Radiology, Harvard Medical School, Boston, MA, USA; [3]Department of Stomatology, School of Dentistry, University of São Paulo, São Paulo, Brazil

Objectives: Susceptibility artefacts from dental materials may compromise MRI diagnosis. However, little is known regarding MRI artefacts of dental material samples with the clinical shapes used in dentistry. The present phantom study aims to clarify how pulse sequences and sequence parameters affect MRI artefacts caused by metal–ceramic restorations.
Methods: A phantom consisting of nickel–chromium metal–ceramic restorations (*i.e.* dental crowns and fixed bridges) and cylindrical reference specimens immersed in agar gel was imaged in 1.5 and 3.0 T MRI scanners. Gradient echo (GRE), spin echo (SE) and ultrashort echo time (UTE) pulse sequences were used. The artefact area in each image was automatically calculated from the pixel values within a region of interest. Mean values for similar pulse sequences differing in one parameter at a time were compared. A comparison between mean artefact area at 1.5 and 3.0 T, and from GRE and SE was also carried out. In addition, a parametric correlation between echo time (TE) and artefact area was performed.
Results: A significant correlation was found between TE and artefact area in GRE images. Higher receiver bandwidth significantly reduced artefact area in SE images. UTE images yielded the smallest artefact area at 1.5 T. In addition, a significant difference in mean artefact area was found between images at 1.5 and 3.0 T field strengths ($p = 0.028$) and between images from GRE and SE pulse sequences ($p = 0.005$).
Conclusions: It is possible to compensate the effect of higher field strength on MRI artefacts by setting optimized pulse sequences for scanning patients with metal–ceramic restorations.
Dentomaxillofacial Radiology (2015) **44**, 20150136. doi: 10.1259/dmfr.20150136

Introduction

New approaches to the application of MRI in dentistry have led to important advances in the field of oral diagnosis.[1–4] MRI provides multiplanar imaging with satisfactory soft-tissue contrast using non-ionizing electromagnetic fields. However, MRI is prone to artefacts caused by the presence of metallic materials, namely susceptibility artefacts, which may preclude a clinical diagnosis or lead to an erroneous diagnosis.[5]

Susceptibility artefacts are generated by magnetic field distortions and signal loss caused by variations in the magnetic field strength that occur on the interface between a dental material and the adjacent tissues.[6,7] The artefact size will vary depending on the shape, orientation, position

and number of objects in or near the imaged volume, as well as the scanner's magnetic field strength, pulse sequence type and pulse sequence parameters.[5,7,8]

Previous studies on neurosurgical materials found significant MRI artefacts from metal alloys such as nickel–chromium and cobalt–chromium in 1.5- and 3.0-T scanners.[9,10] The same metal alloys were also assessed at 1.5 T in two dentistry studies.[11,12] However, the dentistry studies used individual samples with special shapes (*i.e.* cylindrical and spherical) that do not occur in actual dental restorations and tested different commercial brands of materials using only a few different gradient echo [gradient-recalled echo (GRE)] and spin echo (SE) pulse sequences. To our knowledge, little is known regarding the influence of different pulse sequence parameters on artefact dimensions in scans of actual metal–ceramic dental restorations (*i.e.* dental crowns and fixed bridges). Furthermore, it was not possible to find previous reports on the use of the ultrashort echo time (UTE) pulse sequence to assess artefacts from the aforementioned metal alloys. Thus, the aim of this phantom study was to clarify how pulse sequence parameters at 1.5- and 3.0-T field strengths affect MRI artefacts caused by metal–ceramic restorations.

Methods and materials

Samples
Three different samples of metal–ceramic dental restorations were included in the test: one single dental crown, one three-element fixed bridge and one five-element fixed bridge. The three samples were fabricated with the same metal alloy commercial brand (Wironia Light; Bego, Bremen, Germany) and composition (64.5% nickel, 22% chromium, 1% molybdenum, 2.5% other elements). In addition, six reference samples of dental ceramics (Noritake Cerabien CZR dentin A2 lot OE903; Noritake Kizai Co. Ltd, Nagoya, Japan) 10 mm in diameter and 2 mm in height were included, since ceramics have very low magnetic susceptibility and do not yield significant artefacts on MRI.[12]

Phantom
A rectangular plastic container measuring $350 \times 160 \times 40$ mm was used to house the phantom of this study. Briefly, a first layer of hot 1% agar in water was poured into the plastic container as a base, filling half the container volume. The container was covered with plastic wrap and maintained at room temperature for 30 min to allow the gel to form. The samples and reference specimens were then carefully placed over the solid first layer of agar gel to ensure that all objects could be scanned in the same slice. Reference specimens were positioned externally to the metal–ceramic samples, which in turn were positioned close to each other in order to simulate the conditions of a dental arch with multiple metal–ceramic restorations (Figure 1a). The distance between reference specimen and metal–ceramic samples was recorded. A second batch of

agar solution was then prepared and poured carefully into the container to fill it, leaving all samples arrayed in the horizontal midplane of the phantom.

MRI scans
The phantom was scanned with a head coil in two different MRI scanners (1.5 T MAGNETOM® Avanto and 3 T Tim Trio; Siemens Healthcare, Erlangen, Germany). All scans were acquired using the coronal orientation with a field of view of $180 \times 180 \times 180$ mm³ and a matrix of 128×128 pixels. Radiofrequency (RF) pulse and gradient modes were set to "fast", with a phase resolution of 100%. Different pulse sequences were adjusted to be as similar as possible for 1.5 and 3.0 T scans, in order to compare values in bandwidth, number of averages (NEX, or number of experiments), repetition time (TR), echo time (TE) and flip angle. Number of slices, slice thickness and flip angle data were retrieved from the digital imaging and communications in medicine (DICOM) files in the metadata window of an open-source DICOM viewer (OsiriX v. 6.0; Pixmeo, Geneva, Switzerland) and recorded. Images were obtained at 1.5 and 3.0 T using GRE, SE and UTE pulse sequences. All pulse sequence parameters compared are shown in Table 1.

Artefact measurement
Artefacts were measured using the threshold tool available on the ImageJ® software (National Institute of Health, Bethesda, MD). A region of interest enclosing the total area with signal loss from the three metal–ceramic restorations and the artefacts caused by them was generated, following previous methodology.[11] All measurements were performed in the slice containing the six reference specimens (Figure 1b). The threshold was defined according to the histogram of the signal intensities (8-bit pixel values). Minimum, maximum and average pixel values were recorded. An optimized lower threshold value of zero and a higher threshold value of 60 were estimated and set for all measurements. Accordingly, all pixels in the aforementioned range were classified as artefacts and included in the autogenerated region of interest. The software measurement tool was then used to calculate the area of the region of interest in squared centimetres. Since this is an entirely automated and reproducible method, a single observer performed all measurements.

Statistical analysis
Sample size (n = number of artefact images) was determined using Fisher's-test, to detect a minimum linear correlation of $r = 0.6$ and to give the study a power of 80%, at a level of significance of 5%. Normality of GRE measurements was assessed using the Shapiro–Wilk test ($p > 0.05$).

Statistical comparisons between mean artefact areas at 1.5 and 3.0 T, and between GRE and SE were performed using the paired *t*-test. At 3.0 T, similar pulse sequences differing in one parameter at a time were also compared using the paired samples *t*-test (Table 2). This set of experimental variations was carried out to evaluate the sole influence of each parameter on the artefact size.
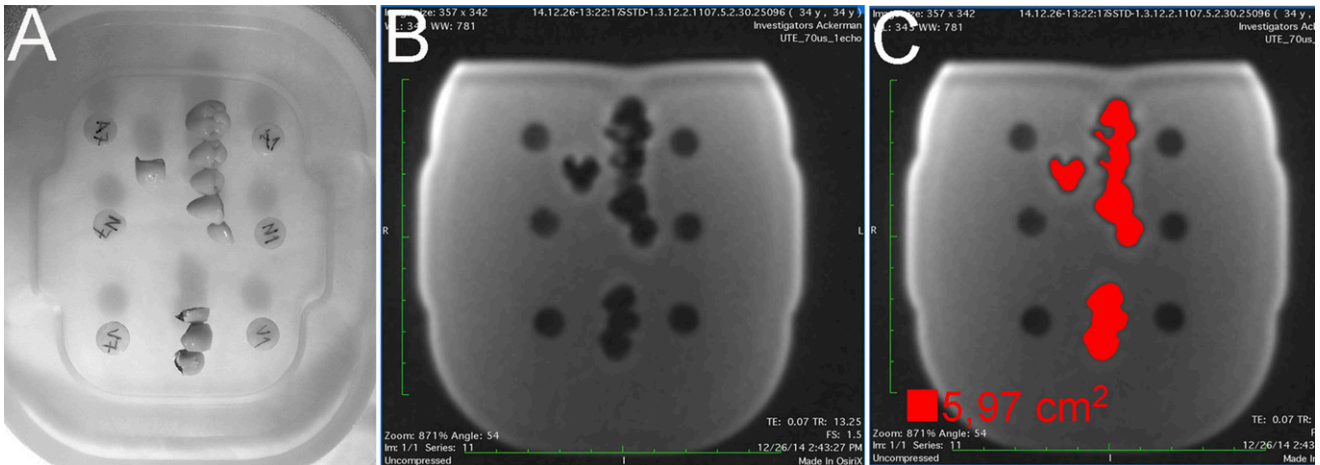
Figure 1 (a) Phantom used in the study. (b) An ultrashort echo time image at 1.5 T of the phantom, which presented the smallest total artefact area. (c) Threshold region-growing method used to perform automated measurements of the total area affected by the artefact. TE, echo time; TR, repetition time.

Alternating parameters include bandwidth, TR, TE, NEX and flip angle. Furthermore, parametric correlation between artefact area and TE was performed for GRE and SE scans performed in the 3.0-T scanner using the Pearson's test. All statistical analyses were performed using the IBM SPSS® Statistics 17 software (IBM Corporation, New York, NY; formerly SPSS Inc., Chicago, IL). A p-value <0.05 was considered statistically significant.

Results

A total of 44 MRI artefact images (10 at 1.5-T field and 34 at 3-T field) were analysed. The mean artefact area of this study was 16.85 ± 8.83 cm^2. The smallest artefact area calculated was 5.97 cm^2 (Figure 1c) obtained using UTE at 1.5 T. Mean artefact area was 21.53 ± 7.80 cm^2 for GRE images, 8.59 ± 2.87 cm^2 for SE images and 6.74 ± 2.52 cm^2 for UTE images.

Normal distribution was confirmed for all measurements according to the Shapiro–Wilk test ($p > 0.05$). A substantial significant increment of artefact area was found between similar pulse sequences at 3.0 T compared with 1.5 T ($p = 0.028$) and for GRE compared with SE ($p = 0.005$) (Figure 2). Furthermore, in GRE images, a longer TR led to small significant reductions ($p = 0.031$) in artefact area, while a shorter TE led to substantial significant reductions ($p = 0.001$). On the other hand,

artefact areas from SE images were only substantially significantly reduced by a higher bandwidth ($p = 0.001$) (Table 2). Finally, a significant parametric correlation between TE and artefact size was found for GRE images ($r = 0.959$; $p = 0.010$) but not for SE images ($p > 0.05$).

Discussion

The advent of MRI in dentistry led to research interest in the interactions of dental materials and RF pulses and magnetic fields. Among the dental materials causing significant MRI artefacts are metal-based materials such as orthodontic brackets and metal–ceramic restorations.[8,12] On the other hand, materials such as ceramics and polymers have low magnetic susceptibility, are compatible with MRI scanning and generally produce minimal or no artefacts.[11,12] Based on this fact, ceramic cylinders were used as reference specimens of the present study.

The size of MRI artefacts caused by different dental materials has been assessed in previous studies using a few pulse sequences to analyse samples of regular shape (*i.e.* cylinders and spheres).[11,12] By contrast with the aforementioned methodology, the present study assessed multiple pulse sequences to analyse nickel–chromium samples with clinical shapes of metal–ceramic restorations. The rationale of testing clinical samples of the same composition with multiple MRI scans was to identify

Table 1 Pulse sequence parameters tested in MRI scans

| Field strength | Type | Pulse sequence parameters | | | | | | |
		Bandwidth (Hz/pixel)	Repetition time (ms)	TE (ms)	Slice thickness (mm)	Number of slices	NEX	Flip angle (degree)
1.5 T	GRE	260	200, 275	3.61, 10, 20	3	10	1	25
	SE	130	275	10, 20	3	10	1	70
	UTE	635	13	0.07	1	192	1	10
3.0 T	GRE	260, 600	275, 600	3.61, 5, 10, 20, 40, 80	3	10	1, 4	50, 30
	SE	130, 601	275, 600	5, 10, 20, 40, 80	3	10	1, 4	115
	UTE	635, 1628	3.16, 600	0.07	1	192	1	10, 15

GRE, gradient echo; NEX, number of experiments (averages); SE, spin echo; TE, echo time; UTE, ultrashort echo time.

Table 2 Mean comparisons performed between similar pulse sequences

Sequence type	Alternating variable	Values compared	Mean difference (cm^2)	p-value[a]
All	Field strength	1.5 T and 3.0 T	5.3 ± 2.0	**0.028**
GRE	Bandwidth (Hz/pixel)	260 and 600	0.3 ± 0.1	0.131
SE	Bandwidth (Hz/pixel)	130 and 601	5.9 ± 0.3	**0.001**
GRE	TR (ms)	275 and 600	0.9 ± 0.4	**0.031**
SE	TR (ms)	275 and 600	0.4 ± 0.3	0.460
GRE	TE (ms)	10 and 20	8.2 ± 0.7	**0.001**
SE	TE (ms)	10 and 20	0.7 ± 0.5	0.371
GRE	NEX	1 and 4	0.2 ± 0.4	0.352
SE	NEX	1 and 4	0.5 ± 0.2	0.122
GRE	Flip angle (degree)	50 and 30	0.2 ± 0.1	0.108

GRE, gradient echo; NEX, number of experiments (averages); SE, spin echo; TE, echo time; TR, repetition time.
[a]Paired sample *t*-test. Significant *p*-values were <0.05 (in bold).

pulse sequence parameters that could be optimized in order to minimize the artefacts. To address the clinical relevance of our methodology, we fabricated a phantom with three different metal–ceramic restorations close to each other, simulating a commonly encountered condition of a patient's dental arch.

Most of the articles in the literature on MRI artefacts have tested materials using different methodologies to estimate the size of the artefacts.[7,9–12] An article on dental materials performed linear measurements of artefacts based on specific threshold limits, following the criteria recommended by the American Society for Testing and Materials (standard F2119-01).[12] These criteria are indicated to estimate the size of an artefact by comparing it with the known actual dimensions of regular shape samples and therefore were not followed in our investigation.

Instead, we measured the entire area with loss of RF signal, which includes the actual metal–ceramic restorations and the artefact caused by their magnetic susceptibility, as performed by similar studies.[10,11] The clinical relevance of this methodology is that larger areas of RF signal loss mean larger areas of misdiagnosed oral tissue. As a result, by testing multiple RF pulse sequences in which single parameters were varied, we were able to define the RF pulse sequence parameters that could be optimized for patients with metal–ceramic restorations, in order to minimize MRI artefacts.

In our comparisons performed at 3.0 T, reducing TE in GRE pulse sequences and increasing bandwidth in SE pulse sequences could reduce artefact size up to 40% for our choice of parameters. These findings are in agreement with a similar study on aneurism clips.[10] A shorter TE results in
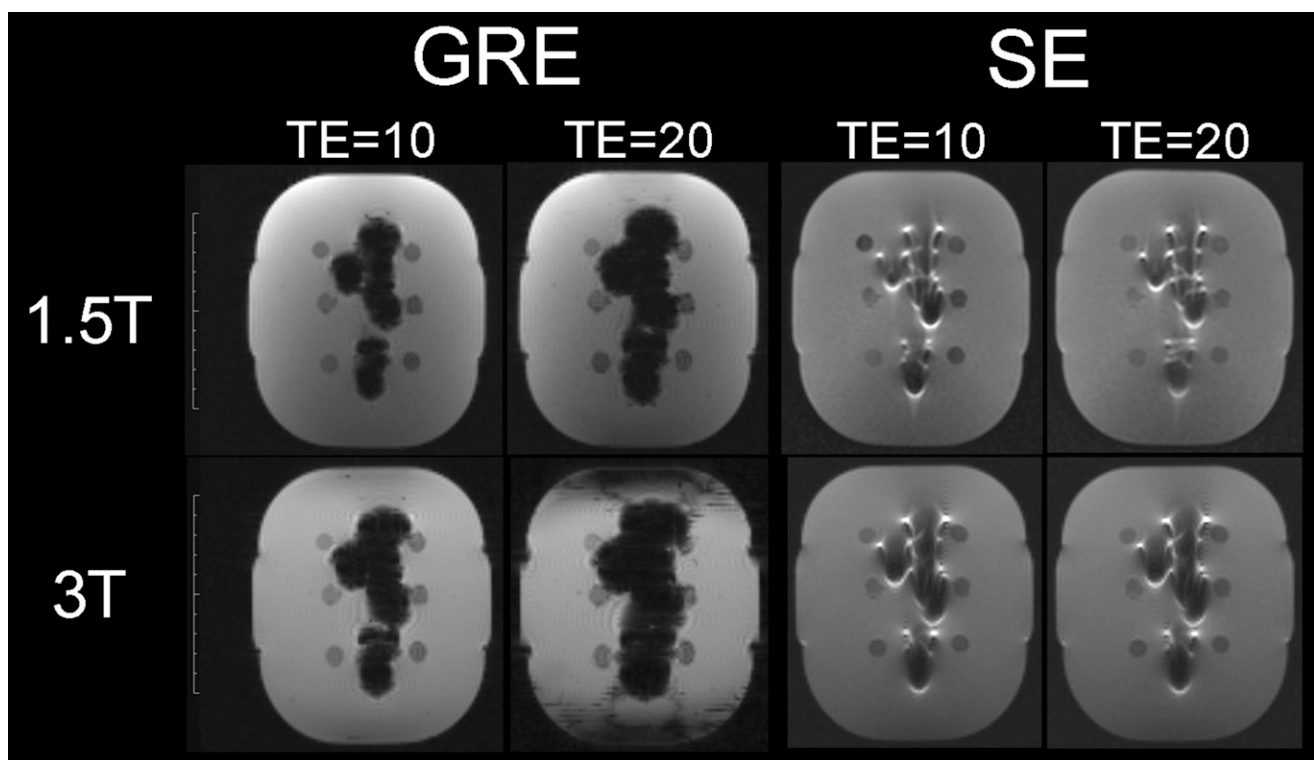

Figure 2 Comparison between gradient echo (GRE) and spin echo (SE) pulse sequences varying in echo time (TE), at 1.5 and 3.0 T. Note that SE images were affected by field strength changes but not by TE changes.

less pixel signal dephasing at the echo peak, leading to less signal loss. A higher bandwidth leads the scanner to apply a larger magnetic field gradient during the frequency encoding period in which the MR signal is digitized, reducing the frequency shift of the artefact relative to the bandwidth per pixel; the artefact therefore occurs over a smaller number of pixels.[13] In addition, a longer TR with other parameters fixed improves image contrast and signal to noise ratio, resulting in small significant area reductions in nickel–chromium artefacts in GRE images. Therefore, TR is a parameter that could be optimized to modestly reduce MRI artefacts, at the expense of a longer scan time.[14]

In our study, while MRI artefacts at 3.0 T were up to 50% larger than at 1.5 T, SE images presented significantly smaller artefacts than GRE images. This finding supports previous studies concluding that GRE pulse sequences are more affected by the presence of metal when compared with SE.[11,15] This is because SE pulse sequences have an 180° RF pulse that refocuses susceptibility-induced frequency shifts at the TE and thereby diminishes the pixel intensity shifts.[16] In addition, SE pulse sequences with higher bandwidth used herein at 3.0 T presented smaller artefacts than UTE images at the same field strength. However, the above-mentioned findings are in contrast to a study concluding that SE could lead to larger artefacts than GRE depending on the magnetic susceptibility of the material.[12]

This is the first study addressing the role of UTE pulse sequences in producing images with reduced size of MRI metal–ceramic artefacts. UTE is a relatively novel method that allows for the visualization of solid structures[17] and has been also described as useful in the field of dentistry.[2,18] Because of its very short TE and use of high bandwidth, it is expected that UTE scans will yield the smallest artefact areas. One limitation of our study, however, is the very restricted choice and range of editable parameters in the pre-commercial UTE pulse sequence provided by the scanner manufacturer, preventing statistical comparisons with general GRE and SE results.

Conclusion

In conclusion, optimization of pulse sequences parameters may significantly reduce susceptibility artefacts caused by nickel–chromium metal–ceramic restorations. In addition, the present results suggest that UTE pulse sequences are suitable to overcome the presence of these artefacts.

Acknowledgments

References

1. Aguiar MF, Marques AP, Carvalho AC, Cavalcanti MG. Accuracy of magnetic resonance imaging compared with computed tomography for implant planning. *Clin Oral Implants Res* 2008; **19**: 362–5. doi: 10.1111/j.1600-0501.2007.01490.x
2. Bracher AK, Hofmann C, Bornstedt A, Hell E, Janke F, Ulrici J, et al. Ultrashort echo time (UTE) MRI for the assessment of caries lesions. *Dentomaxillofac Radiol* 2013; **42**: 20120321. doi: 10.1259/dmfr.20120321
3. Nagamatsu-Sakaguchi C, Maekawa K, Ono T, Yanagi Y, Minakuchi H, Miyawaki S, et al. Test-retest reliability of MRI-based disk position diagnosis of the temporomandibular joint. *Clin Oral Investig* 2012; **16**: 101–8. doi: 10.1007/s00784-010-0476-9
4. Senel FC, Duran S, Icten O, Izbudak I, Cizmeci F. Assessment of the sinus lift operation by magnetic resonance imaging. *Br J Oral Maxillofac Surg* 2006; **44**: 511–14. doi: 10.1016/j.bjoms.2006.02.004
5. Schenck JF. The role of magnetic susceptibility in magnetic resonance imaging: MRI magnetic compatibility of the first and second kinds. *Med Phys* 1996; **23**: 815–50. doi: 10.1118/1.597854
6. Beuf O, Lissac M, Crémillieux Y, Briguet A. Correlation between magnetic resonance imaging disturbances and the magnetic susceptibility of dental materials. *Dent Mater* 1994; **10**: 265–8. doi: 10.1016/0109-5641(94)90072-8
7. Bui FM, Bott K, Mintchev MP. A quantitative study of the pixel-shifting, blurring and nonlinear distortions in MRI images caused by the presence of metal implants. *J Med Eng Technol* 2000; **24**: 20–7.
8. Hubálková H, Hora K, Seidl Z, Krásenský J. Dental materials and magnetic resonance imaging. *Eur J Prosthodont Restor Dent* 2002; **10**: 125–30.
9. Matsuura H, Inoue T, Ogasawara K, Sasaki M, Konno H, Kuzu Y, et al. Quantitative analysis of magnetic resonance imaging susceptibility artifacts caused by neurosurgical biomaterials: comparison of 0.5, 1.5, and 3.0 Tesla magnetic fields. *Neurol Med Chir (Tokyo)* 2005; **45**: 395–8; discussion 398–9. doi: 10.2176/nmc.45.395

10. Olsrud J, Lätt J, Brockstedt S, Romner B, Björkman-Burtscher IM. Magnetic resonance imaging artifacts caused by aneurysm clips and shunt valves: dependence on field strength (1.5 and 3 T) and imaging parameters. *J Magn Reson Imaging* 2005; **22**: 433–7. doi: 10.1002/jmri.20391
11. Klinke T, Daboul A, Maron J, Gredes T, Puls R, Jaghsi A, et al. Artifacts in magnetic resonance imaging and computed tomography caused by dental materials. *PLoS One* 2012; **7**: e31766. doi: 10.1371/journal.pone.0031766
12. Starcuková J, Starcuk Z Jr, Hubálková H, Linetskiy I. Magnetic susceptibility and electrical conductivity of metallic dental materials and their impact on MR imaging artifacts. *Dent Mater* 2008; **24**: 715–23.
13. Lüdeke KM, Röschmann P, Tischler R. Susceptibility artefacts in NMR imaging. *Magn Reson Imaging* 1985; **3**: 329–43.
14. Li T, Mirowitz SA. Fast multi-planar gradient echo MR imaging: impact of variation in pulse sequence parameters on image quality and artifacts. *Magn Reson Imaging* 2004; **22**: 807–14. doi: 10.1016/j.mri.2004.01.051
15. Stradiotti P, Curti A, Castellazzi G, Zerbi A. Metal-related artifacts in instrumented spine. Techniques for reducing artifacts in CT and MRI: state of the art. *Eur Spine J* 2009; **18**(Suppl. 1): 102–8. doi: 10.1007/s00586-009-0998-5
16. Lee MJ, Kim S, Lee SA, Song HT, Huh YM, Kim DH, et al. Overcoming artifacts from metallic orthopedic implants at high-field-strength MR imaging and multi-detector CT. *Radiographics* 2007; **27**: 791–803. doi: 10.1148/rg.273065087
17. Reichert IL, Robson MD, Gatehouse PD, He T, Chappell KE, Holmes J, et al. Magnetic resonance imaging of cortical bone with ultrashort TE pulse sequences. *Magn Reson Imaging* 2005; **23**: 611–18. doi: 10.1016/j.mri.2005.02.017
18. Hövener JB, Zwick S, Leupold J, Eisenbeiß AK, Scheifele C, Schellenberger F, et al. Dental MRI: imaging of soft and solid components without ionizing radiation. *J Magn Reson Imaging* 2012; **36**: 841–6. doi: 10.1002/jmri.23712